DESIGN, ANALYSIS AND PROTOTYPING OF ACTIVE TAB ROTOR

KOBIKI Noboru, Yasutada TANABE, Takashi AOYAMA, JAXA, Tokyo, Japan
Do-Hyung Kim, Hee Jung Kang, Seong-Yong Wie, Seung-Ho Kim, KARI, Daejeon, Korea

Abstract

JAXA (Japan Aerospace Exploration Agency) and KARI (Korea Aerospace Research Institute) jointly started the activities related to the research and development of Active Tab as the helicopter noise reduction technique. KARI constructed the analytical methodology consisting of the aerodynamic, structural dynamic and acoustic codes for defining the requirements for and evaluation of the performances of Active Tab installed in a Mach scaled assumed blade. Based on the defined requirements, JAXA carried out the conceptual design study, developed and evaluated the performances of the Active Tab drive mechanism. The analytical results show Active Tab satisfying the requirements has the sufficient noise reduction capability. The evaluation for the Active Tab drive mechanism demonstrated the dynamic performance and durability available for the practical use installed in helicopter blades.

1. INTRODUCTION

Among the noises generated by helicopters, the Blade-Vortex Interaction (BVI) noise causes significant damage and cannot be well reduced by passive techniques such as airfoil/tip shape improvement. In order to resolve this BVI noise problem, many research organizations and helicopter manufactures have been working to research/develop BVI noise reduction techniques for these decades as one of the high priority technical tasks.

Several active techniques, such as HHC (Higher Harmonic Control) [1-5], IBC (Individual Blade Control) [6-9], Active Flap [10-15], Active Twist [16-18] and the like, have been proposed, researched and developed for helicopter noise/vibration reduction so far. Some of them were flight-tested and others are in the phase just close to flight test evaluation.

JAXA (Japan Aerospace Exploration Agency) and Kawada Industries Inc. have been working to research and develop a new active technique for helicopter noise reduction which is available to ICAO defined flight patterns, namely approach, fly over and take-off [19].

The schematic view of Active Tab is shown in Fig.1. Active Tab is installed in the aft portion of the airfoil and driven back and forth dynamically to reduce BVI noise and the vibration by the blade circulation control due to the variable blade area effect with the aim of the low power consumption. Active Tab also can be operated statically, such as the active tab is deployed with some displacement and fixed. This way of operation can increase the blade lift during the whole revolution of the blade so that the rotor speed can be reduced by making use of this lift increment, which has the reduction effect not only on the approach/landing noise (BVI noise), but also on the climb and fly-over noises.

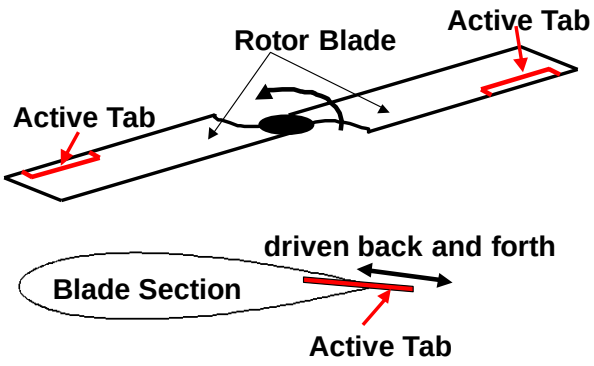

Figure 1: Active Tab concept

JAXA (Japan Aerospace Exploration Agency) and KARI (Korea Aerospace Research Institute) jointly started the activities related to the research and development of active technologies for helicopter noise reduction in 2009 to provide the technical solutions to the above mentioned problem. Both of the parties agreed on Active Tab as the target active technique of this joint research program.

The basic research for Active Tab had been carried out by JAXA and Kawada Industries Inc. by using a 1-bladed rotor system on a low tip speed (62.8m/sec) condition [20-22]. It is demonstrated by this phase of the study in a rotor configuration that Active Tab had the efficient capability to control the

rotor noise and that Active Tab is one of the promising techniques for rotor noise reduction.

As the next step, JAXA/KARI joint research program is established to demonstrate Active Tab capability by using a 2-bladed rotor system on a Mach scaled condition.

In the framework of this joint research program, KARI has the responsibility to provide an existing rotor system with newly designed blades in which Active Tab can be installed. On the other hand, JAXA does to develop a drive mechanism of Active Tab. Both of the parties develop the analytical methods to evaluate the noise reduction capability of Active Tab Rotor.

This paper describes the research process of the Active Tab rotor consisting of the developments for analytical methodology and Active Tab hardware.

Active Tab for the Mach scaled blade are defined and its schematic drawing is shown in Fig.2.

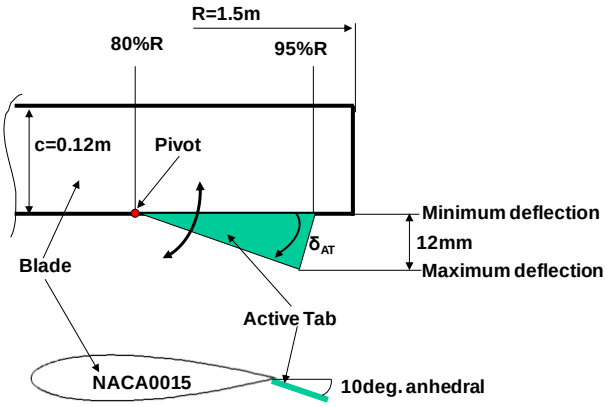

Figure 2: Active Tab installation [23]

2. ACTIVE TAB ROTOR MODELING

In order to analyze the effect of Active Tab on the aeroacoustic characteristics, CAMRAD II model was prepared and the airloads were predicted, then BVI noise characteristics were calculated.

2.1. Rotor System

A 2-bladed model rotor system with 1.5 m radius and a teetering hub was designed for implementing Active Tab considering the size of Active Tab drive mechanism and the capability of the rotor test stand. The general properties of the model rotor system are given in Table 1.

Table 1: Rotor properties

Properties	Values
No. of blades	2
Hub type	teetering
Rotating direction	counter clockwise
Rotating speed	1,300 rpm
Radius	1.5 m
Chord length	0.12 m
Airfoil	NACA0015
Twist	-8 deg. Linear
Root cut-out	0.17 R

2.2. Active Tab

Based on the achievement of wind tunnel tests by a one-bladed rotor system [20,21], the features of Active Tab for the Mach scaled blade are defined and its schematic drawing is shown in Fig.2.

The tab is fan-shaped so that the extended area generated by the tab operation is made larger in the outer portion of the blade where the dynamic pressure is higher than that in the inner portion. A 10deg. anhedral angle is put to the tab so that the tab effect to the blade lift increment is augmented. This Active Tab is pivoted at its apex to 80%R location of the blade. NACA0015 is selected as the airfoil of the blade in order to provide as large thickness to store the drive mechanism of Active Tab as possible without significant disadvantage to the maximum lift of the blade.

For simple consideration of the effect of Active Tab, it is modeled as rectangular instead of fan-shaped as shown in Fig. 3. Additional airfoil tables with different tab chord length were generated for the sections from 0.8R to 0.95R; which was implemented in CAMRAD II model.

The Active Tab drive mechanism is composed of a piezoelectric actuator and mechanical parts amplifying the amplitude of the actuator displacement and transmitting the actuator output into the motion of Active Tab. The driving mechanism is installed inside the blade, and the inertial properties are modeled as a lumped mass in the structural part of CAMRAD II model. The inertial properties of the driving mechanism are shown in Table 2.

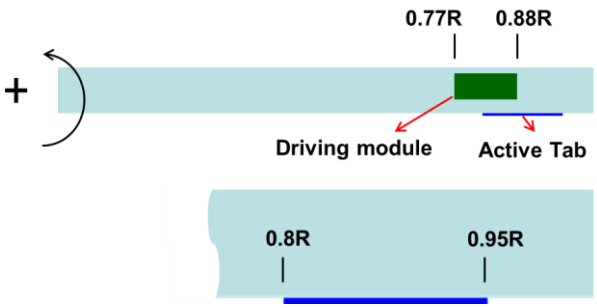

Figure 3: Tab location

Table 2: Inertial properties of driving module

Properties	Values
Mass	360 g
Moment of Inertia	1.71×10^{-4} kgm^2
Center of gravity	0.84R / 0.3749c

2.3. Construction of Aerodynamic Tables for Airfoil with Tab

The analysis of Active Tab rotor using CAMRAD II needs aerodynamic tables for airfoil with tab, which should be considered the tab chord length to simulate the Active Tab rotor.

Aerodynamic tables for flow conditions of the airfoil with the angle of attack range from -16 degrees to +16 degrees and the Mach number range from 0.1 to 1.0 were constructed by using the Fluent of ANSYS software. The numerical calculation for lift, drag and moment coefficients of the airfoil with tab was performed for the range of the tab chord length from 0 to 12mm with 2mm interval.

The density-based RANS (Reynolds Average Navier-Stokes) flow solver with Roe's flux-difference splitting with the least-square reconstruction for the 2nd order scheme in the Fluent was used. The effect of turbulent is estimated by the Spalart-Allmaras one-equation model.

The pressure far-field boundary condition at the far-field was placed at 30 times of the airfoil chord length and the no-slip condition on the airfoil surface was applied. Fig. 4 (a) shows the computational mesh distribution around the airfoil and Fig. 4 (b) does that around the tab. Meshes around airfoil surface and behind the trailing-edge were refined to resolve the viscous effect and the wake. The 25-layers prism mesh was also applied on the airfoil surface.

For the high angle of attack range, aerodynamic tables were constructed by using the analytic model described in Ref.5.

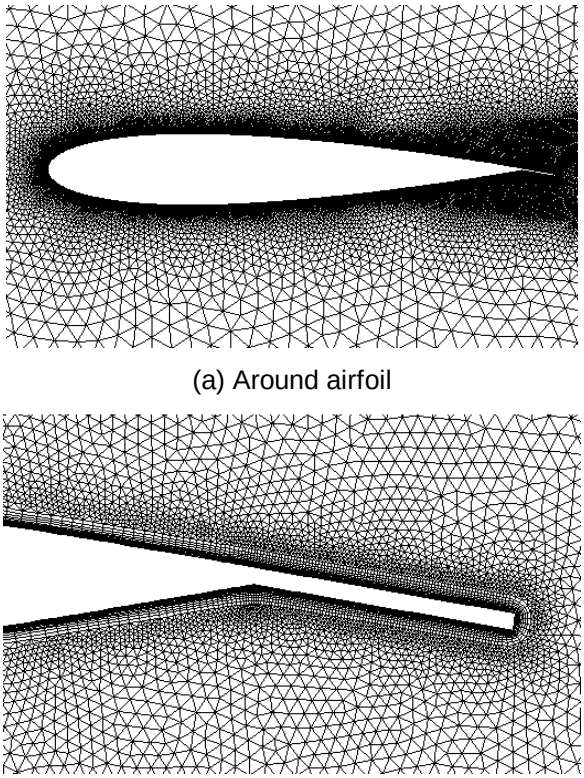

(a) Around airfoil

(b) Around tab

Figure 4: Computational mesh distribution around the airfoil and tab

2.4. Blade

The model blade was designed according to the procedure shown in Fig. 5. In order to produce sufficient elastic torsion deformation produced by the Active Tab actuation, the target torsion frequency was selected to be close to 4/rev.

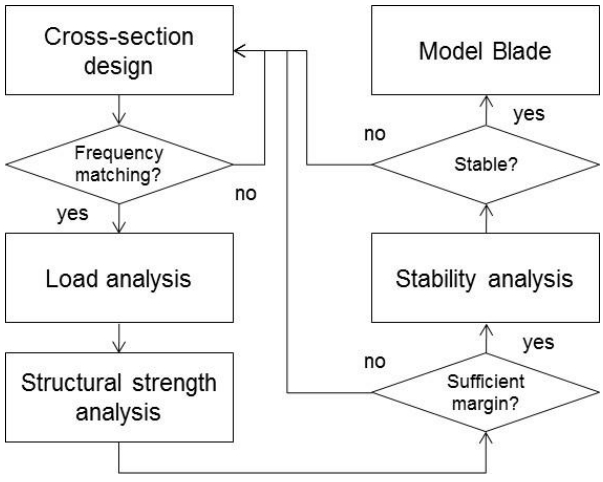

Figure 5: Blade design procedure

2.4.1. Cross Section Design

Three sections of the blade with D-shape spar were designed and transition region was generated by interpolation. The typical section for the main lifting area is shown in Fig. 6. The primary materials for blade structure are carbon fabric/epoxy prepreg, unidirectional carbon/epoxy prepreg, and tungsten rods are used for weight balance. Mainly [0/90] stacking angle is utilized for realizing relatively low first torsion frequency. KARI's in-house program, CORDAS (Composite Rotor blade Design and Analysis Software) was used for design and analysis of the blade cross sections.

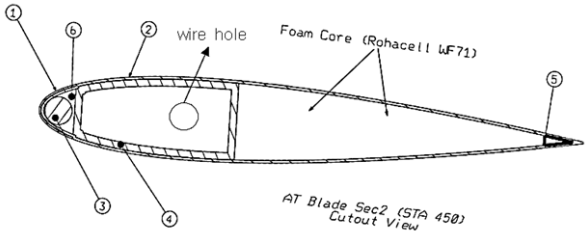

① nose skin : [0/90] carbon fabric 2-plies
② skin: [0/90] carbon fabric 3-plies
③ balance weight: tungsten rod 6 mm diameter
④ spar : [0/90] carbon fabric 8-plies
⑤ TE stiffener: [0] UD carbon
⑥ LE stiffener: [0] UD carbon

Figure 6: Typical section view

2.4.2. Dynamic Analysis

For checking the frequency placement of the blade, the fan-plot analysis was performed. The first torsion frequency is close to 4/rev as shown in Fig. 7. Although the first lead-lag mode showed very low modal damping, the aeroelastic instability was not observed on the hover conditions with collective pitch variations as shown in Fig. 8.

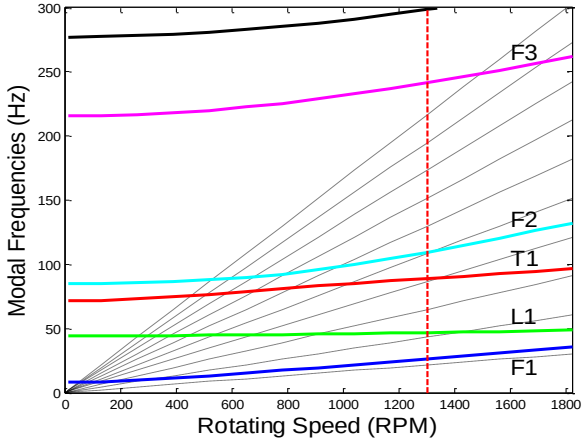

Figure 7: Fan-plot of the designed blade

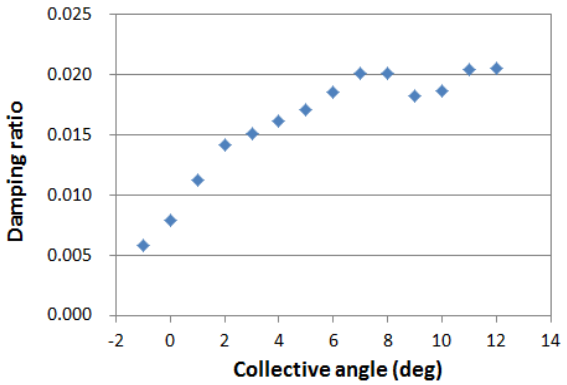

Figure 8: First lag mode damping in hover

2.4.3. Load Analysis

The blade load analysis was performed at hover, forward flight with advance ratio 0.25, and descent flight with advance ratio 0.15. Fig. 9 shows the blade spanwise load distribution at forward flight which produced the biggest structural load among three flight conditions. Discontinuous load distribution can be seen in the structural element which includes Active Tab drive mechanism as a lumped mass and large bending moments are acting at the inboard region.

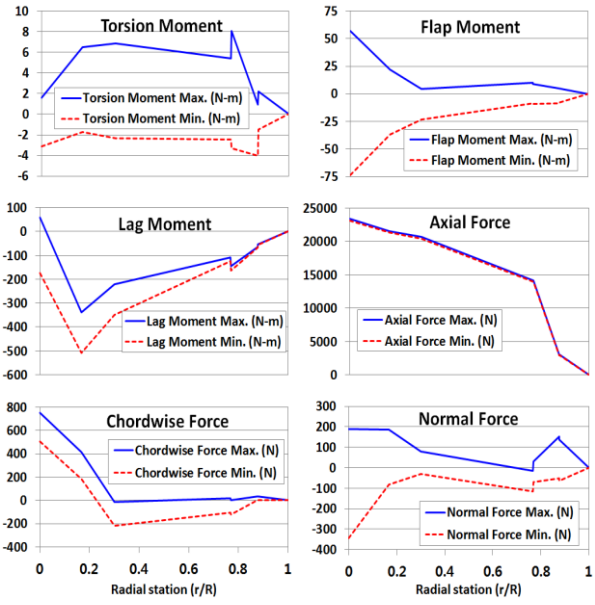

Figure 9: Blade load distribution (fwd flight)

2.4.4. Strength Analysis

The maximum strain was calculated at skin using the combined load composed of axial force, flap

and lag moments. Then structural safety factor was calculated based on the design allowable strain of the material. The ultimate load was applied as 1.5 times of the limit load, and 70% of the failure strain was used as the design allowable strain [25].

The calculated minimum safety factors for hover, level flight (μ=0.25), and descent (μ=0.15) were 3.27, 2.96, and 3.21, respectively. Therefore the blade itself has the sufficient static structural strength.

3. EVALUATION OF AERODYNAMIC AND ACOUSTIC CHARACTERISTICS

The airloads prediction was performed using CAMRAD II, and then the noise level was evaluated using an in-house program. The multiple trailers with the consolidation option was used for the wake model and ONERA EDLIN model [26] was used for the unsteady aerodynamic load calculation. The post-trim was applied to get 2 degree azimuthal step high resolution airloads data.

3.1. Rotor Trim

Three variable propulsive trim was applied with the three trim targets thrust (Fz), propulsive force (Fx), and zero rolling moment (Mx = 0) and the shaft was fixed to a specified angle. It is time saving approach compared with the four variable trim (trim targets Fz, Fx, Mx = My = 0) in the wind tunnel test [27]. Three control inputs θ_0, θ_{1C}, and θ_{1S} are used to match three targets. Three variable propulsive trim has an advantage of having matched propulsive force, however large longitudinal flapping can be produced if the shaft tilt angle is not properly set up.

3.2. Acoustic Analysis Methodology

For rotor noise prediction, the Farassat formulation 1A [28] based on the Ffowcs-Williams Hawkings (FW-H) equation is used. The Farassat formulation is implemented using the monopole and dipole noise terms and the each term represents thickness and loading noise, respectively. To consider the retarded time calculation, the source-time dominant algorithm and the wind effect correction were applied to the acoustic analysis code.

The input (airload and blade deformation information) for the acoustic analysis was calculated by CAMRADII. Using acoustic analysis code, the acoustic pressure signal and Sound Pressure Level (SPL) were calculated at observer positions.

Fig. 10 shows the map for noise calculation. It is located 1.1R below the hub center with 3R by 4R area. The positive direction of each axis is the downstream wind direction (X), the starboard (Y), and the lift direction (Z).

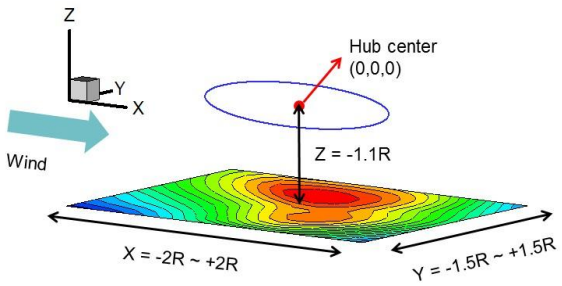

Figure 10: Noise calculation map

The BVI noise can be identified as the mid-frequency contents in noise spectra as shown in Fig. 11. It is dominant at descent flight condition, and suitable frequency range can be distinguished by comparing noise spectra of the descent and other flight conditions.

The noise spectrum of the descent flight (advance ratio 0.15, shaft tilt angle 7.1 degree) is compared with the level flight with the same flight speed (advance ratio 0.15, shaft tilt angle -1.9 degree) in Fig. 12. SPLs at the same location (X = -0.25R, Y = 0.75 R, Z = -1.1R) show that the levels of low-frequency loading noise are almost same but the strong noise contents can be found in the mid-frequency range at the descent flight condition. The frequency range of this area is 5~48 bpf (blade passing frequency) and SPL due to this frequency range is denoted as BVISPL (Blade Vortex Interaction Sound Pressure Level).

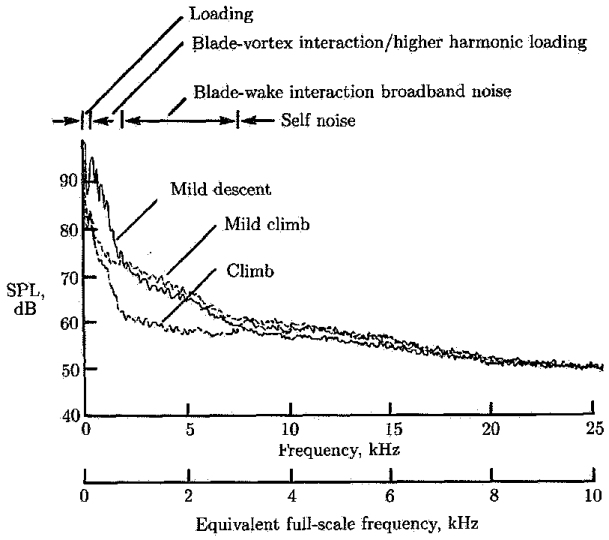

Figure 11: Typical overhead noise spectra of 2/5-scale BO-105 model rotor [29]

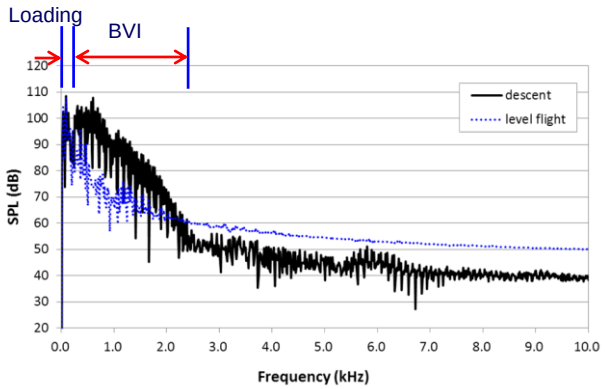

(a) Noise spectra (linear scale)

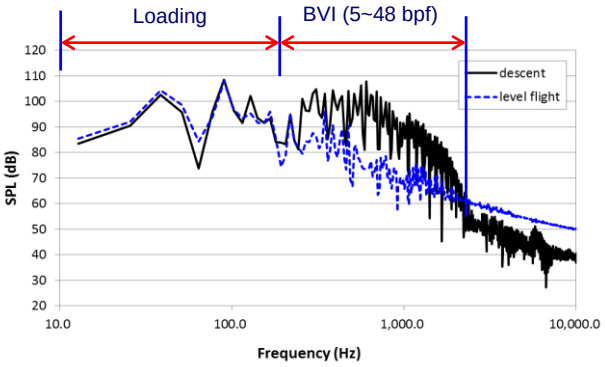

(b) Noise spectra (log scale)

Figure 12: Comparison of noise spectra at descent and level flight condition

3.3. Baseline Flight Condition

Maximum BVI noise condition was selected as the baseline flight condition in order to clearly bring out the effect of Active Tab on BVI noise reduction. The shaft angle sweep was performed at descent flight with the same wind speed 31 m/s (advance ratio 0.15). The airframe drag and the rotor drag were considered for setting the shaft tilt angle. The equivalent flat plate area of the rotor test stand was used for the airframe drag (Fx = 59 N) calculation and the mean airfoil drag was used for rotor drag (H = 8 N). The target thrust was selected to match the scaled weight of AH-1G with the scale factor of 4.47, which is W = 1,473 N. The computation was performed at various shaft angles listed in Table 3 with thrust, propulsive force, and zero rolling moment trim targets.

The maximum SPL of each case in Table 3 is compared in Fig. 13. The maximum OASPL (Overall SPL) and BVISPL are seen at the shaft tilt angle 7.1 degree; which is selected as the baseline (BL) condition.

Table 3: Shaft angle sweep conditions

Flight path angle (deg)	Shaft tilt angle (deg)	Trim target	
		CH/σ	CT/σ
5	3.1	4.38396E-04	7.99306E-02
6	4.1	4.38396E-04	7.98916E-02
7	5.1	4.38396E-04	7.98526E-02
8	6.1	4.38396E-04	7.98137E-02
9	7.1	4.38396E-04	7.97749E-02
10	8.1	4.38396E-04	7.97361E-02

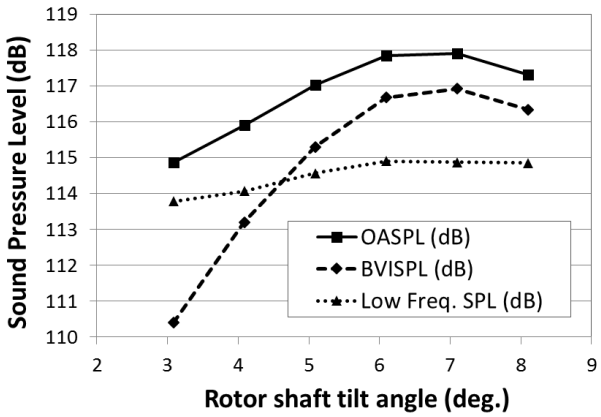

Figure 13: SPL variations with respect to rotor shaft tile angle.

4. PROTOTYPE DEVELOPMENT FOR ACTIVE TAB DRIVE MECHANISM

4.1. Requirements

Based on the experimental results [20, 21] and the analytical prediction, the requirement for Active Tab is set up as follows.

Active Tab :
- Span length : 80-95%R
- Displacement : 12mm
- Frequency : 2/rev (43.3Hz)
- with 20N simulated lift acted on tab

Instrumentation :
- Active Tab displacement
- Hinge moment
- Output displacement of the double armed amplifier
- Actuator displacement
- Input voltage to actuator

The inertial properties of the driving mechanism described in Table 2 are the requirements as well.

4.2. Conceptual Study

A conceptual design study of Active Tab in order to be installed in a Mach scaled assumed blade is carried out [30]. Then, the prototype of the drive mechanism of Active Tab shown in Fig.14 is developed based on this conceptual design study [23, 31, 32].

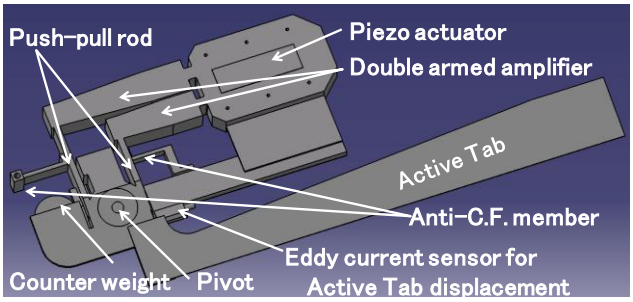

Figure 14: Active Tab drive mechanism [23]

A single stacked piezo actuator stored in a casing generates a linear reciprocal movement, which is magnified by the double armed amplifier and transformed into a rotary displacement of the arms around the pivot. Then, Active Tab is driven via a pivot in a rotational reciprocal direction. A counter weight is connected on the opposite side of Active Tab across the pivot in order to cancel the centrifugal force acting about the pivot.

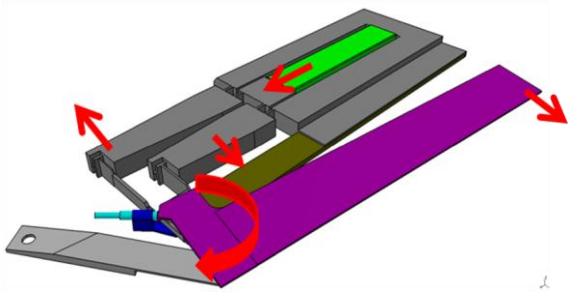

(a) Active Tab spreading process

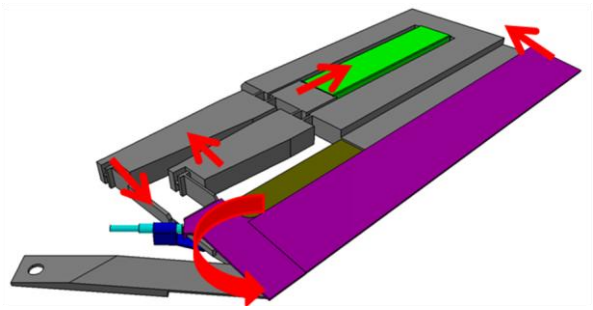

(b) Active Tab retrieving process

Figure 15: Active Tab deployment sequence [23]

The sequence of Active Tab deployment is shown in Fig.15. The process of Active Tab spreading is depicted in Fig.15 (a). At first, the piezo actuator (green part) extends. This movement opens apart each arm (gray parts) of the amplifier, which generates a torque around the pivot in the direction of making Active Tab (purple part) rotationally spreading around the pivot. The opposite happens in the retrieving process which is initiated by the piezo actuator shrinking as depicted in Fig. 15 (b).

4.3. System Design and Development

The Active Tab drive mechanism is developed as shown in Fig.16 which is geometrically suitable to the assumed blade and satisfies the requirements described in 4.1.

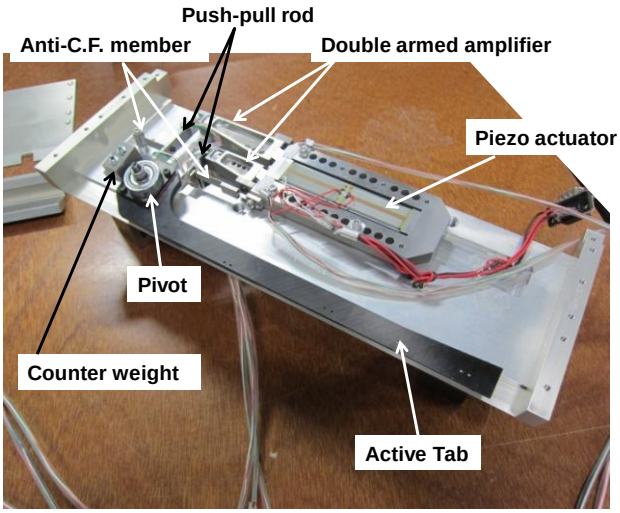

Figure 16: Finalized Active Tab drive mechanism with simulated blade [23]

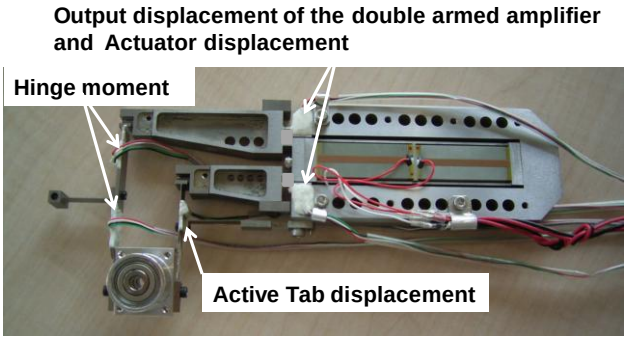

Figure 17: Strain gauge position for instrumentation [23]

All the measurements other than the input voltage to the actuator are measured by strain gauges in the Active Tab drive mechanism. The position of the strain gauge for each measuring item is shown in Fig.17.

The unsteady Active Tab displacement is measured by the strain gauge on the shorter push-pull rod. The hinge moment is measured by those on the longer push-pull rod, the output displacement of the double armed amplifier and the actuator displacement are done by those on the base portion of the double armed amplifier.

5. RESULTS AND DISCUSSION

5.1. BVI Noise at Baseline Condition

The blade section normal force distribution is shown in Fig. 18. The fluctuation of the normal force is found in advancing and retreating sides due to BVI. Fig. 19 is BVISPL noise map of the baseline condition. The maximum BVISPL can be found in the second quadrant and the direction of BVI noise propagation is about 110 degree.

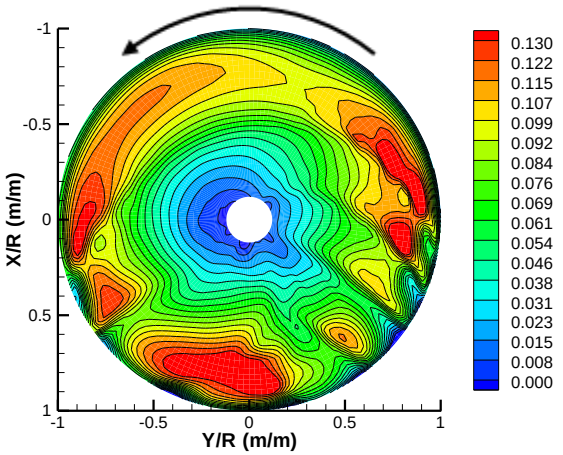

Figure 18: Section normal force (M^2C_n, BL)

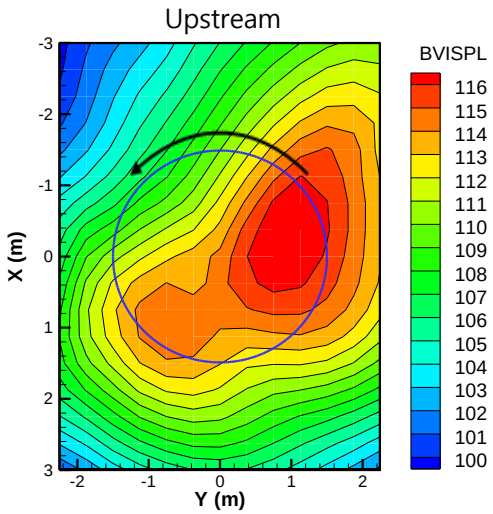

Figure 19: Noise map (BVISPL, BL)

5.2. Active Tab Effect on BVI Noise

The variations of the BVISPL were investigated by applying HHC (Higher Harmonic Control) actuation of Active Tab. The displacement of Active Tab is defined as follows:

$$A = \frac{A_n}{2} + \frac{A_n}{2}\cos(n\varphi - \varphi_n), (n = 2, 3)$$

where, A is the tab displacement extracted from the trailing edge of the blade, A_n is commanded amplitude, n is the order of harmonics, φ is the azimuth angle, and φ_n is the control phase angle. In the present study, the characteristics of the BVI noise were investigated using n = 2, 3 (2/rev and 3/rev) HHC actuations with A_n = 3, 6, 9, 12 mm and φ_n = 0 to 330 degrees with 30 degree interval.

For 2/rev actuation, BVISPL changes with respect to the Active Tab amplitude and the control phase angle are shown in Fig. 20. Maximum BVISPL is reduced with control phase angles 150 ~ 30 degrees. BVISPL also changed according to the control amplitude, but the waveforms with different amplitudes are similar. The minimum noise condition was found at A_n = 6 mm amplitude and φ_n = 270 degree control phase. The amount of BVISPL reduction is 2.0 dB.

The blade section normal force distribution for the minimum noise condition with 2/rev actuation is shown in Fig. 21 and the noise map is shown in Fig. 22. The fluctuation of the normal force is alleviated in the advancing side and the location of peak BVISPL is observed in 60 degree azimuthal direction.

For 3/rev actuation, BVISPL changes are shown in Fig. 23. The BVI noise reduction can be achieved with control phase angles 270 ~ 120 degrees. The minimum noise condition was found at A_n = 6 mm amplitude and φ_n = 30 degree control phase. The amount of BVISPL reduction is 3.3 dB.

The blade section normal force distribution for the minimum noise condition with 3/rev actuation is shown in Fig. 24 and the noise map is shown in Fig. 25. Fluctuation of normal force is much more smoothed in the advancing side. The direction of peak BVISPL location is similar to the minimum noise condition with 2/rev actuation, but the maximum BVISPL is reduced by 3.3 dB which is 1.3 dB higher gain than 2/rev actuation. Therefore 3/rev actuation is more effective within the present calculation ranges.

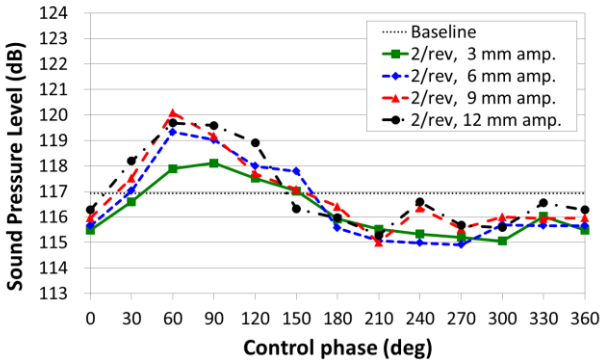

Figure 20: Max. BVISPL variations (2/rev actuation)

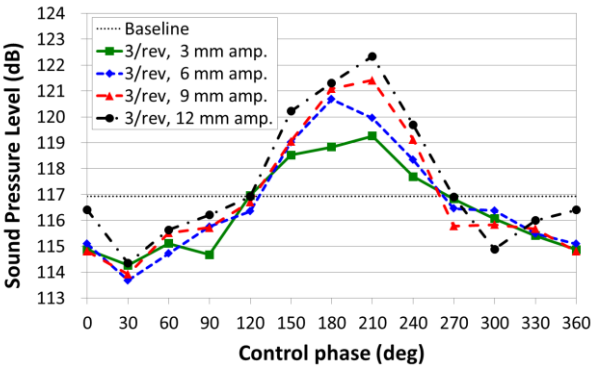

Figure 23: Max. BVISPL variations (3/rev actuation)

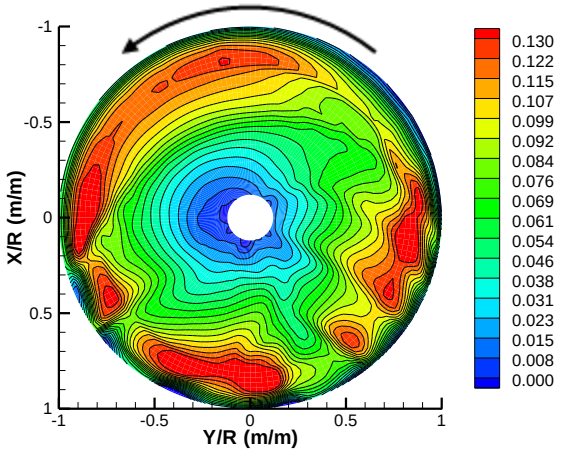

Figure 21: Section normal force (M^2C_n, MN-2P, A_n = 6 mm, φ_n = 270 degree)

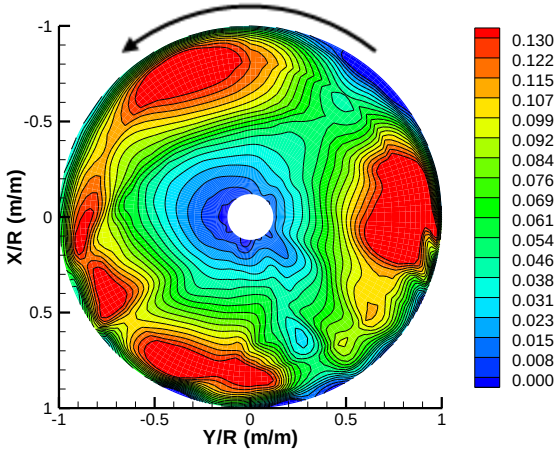

Figure 24: Section normal force (M^2C_n, MN-3P, A_n = 6 mm, φ_n = 30 degree)

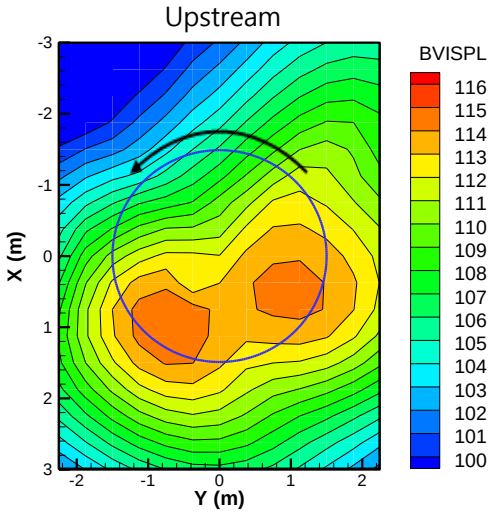

Figure 22: Noise map (BVISPL, MN-2P, A_n = 6 mm, φ_n = 270 degree)

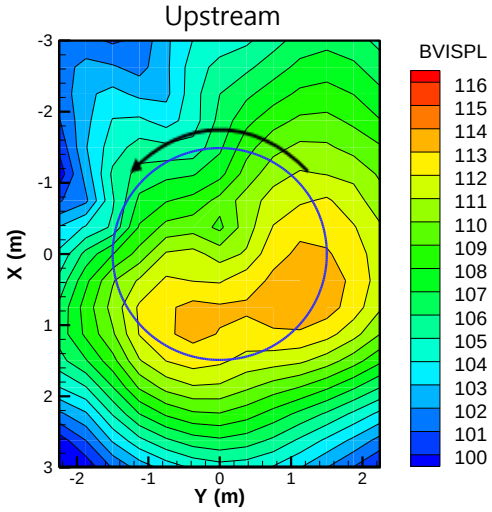

Figure 25: Noise map (BVISPL, MN-3P, A_n = 6 mm, φ_n = 30 degree)

5.3. Performance of Active Tab Drive mechanism

The two types of tests, namely a dynamic test and an endurance test, are conducted to examine and demonstrate the performance of the drive mechanism.

5.3.1. Dynamic test

Fig.26 shows the set up of the dynamic test. The endurance test described later is also carried out by this set up.

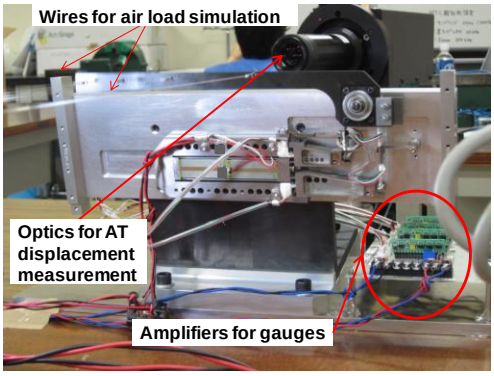

Fig.26: Set up of dynamic and endurance tests [23]

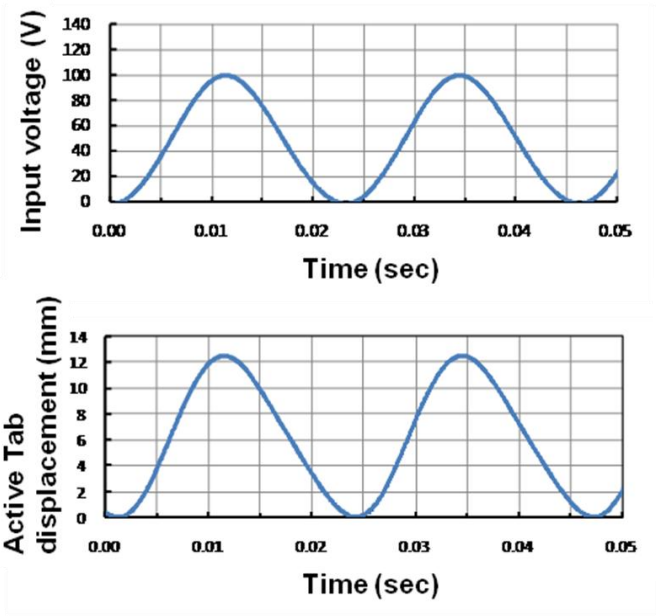

(a) Active Tab displacement and input voltage :time history
0: Active Tab is completely retrieved.
+: Active Tab is deployed.

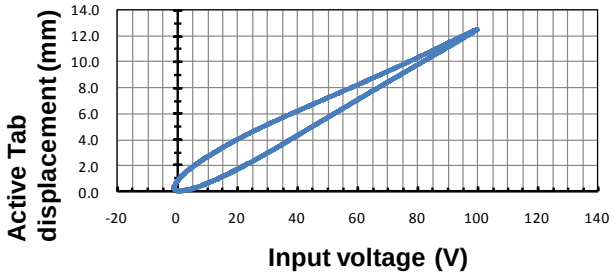

(b) Hysteresis of Active Tab displacement with respect to input voltage

Figure 27: Dynamic characteristics of Active Tab drive mechanism [23]

Input voltage=50V+/-50V
Active Tab frequency=2/rev (43.3Hz)
with 20N simulated lift acted on tab

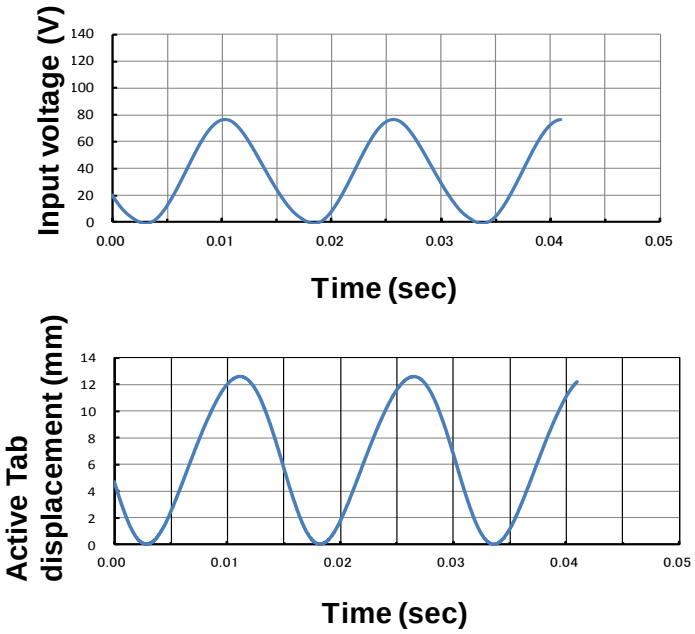

(a) Active Tab displacement and input voltage :time history
0: Active Tab is completely retrieved.
+: Active Tab is deployed.

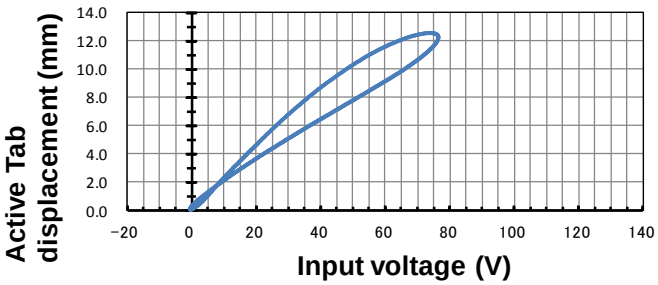

(b) Hysteresis of Active Tab displacement with respect to input voltage

Figure 28: Dynamic characteristics of Active Tab drive mechanism

Input voltage=40V+/-40V
Active Tab frequency=3/rev (65.0Hz)
with 20N simulated lift acted on tab

The dynamic test is carried out to evaluate the operability of Active Tab drive mechanism on the target condition. For this objective, Active Tab drive mechanism is operated with input voltage 50V+/-50V at 2/rev (43.3Hz) and 40V+/-40V at 3/rev (65.0Hz) with 20N simulated lift acted on tab.

Fig.27 shows the dynamic test result for 2/rev cases and Fig.28 does for 3/rev ones. These figures denote the dynamic behavior of Active Tab drive mechanism measured by the generated displacement of Active Tab with simultaneously measured input voltage to the actuator. As shown in Fig.27 (a) and Fig.28 (a), the 12mm displacements of Active Tab drive mechanism are obtained, which satisfies the requirement mentioned above.

Fig.27 (b) and Fig.28 (b) show the hysteresis characteristics of Active Tab displacement with respect to input voltage. This hysteresis can be coped with the feedback controls to eliminate during the practical use of Active Tab in the blade.

5.3.2. Endurance test

The endurance test is to demonstrate the durability of the drive mechanism and to examine the heat accumulating characteristics with respect to the operation time.

For this test, Active Tab drive mechanism is continuously operated with input voltage 50V+/-50V at 43.3Hz with 20N simulated lift acted on tab.

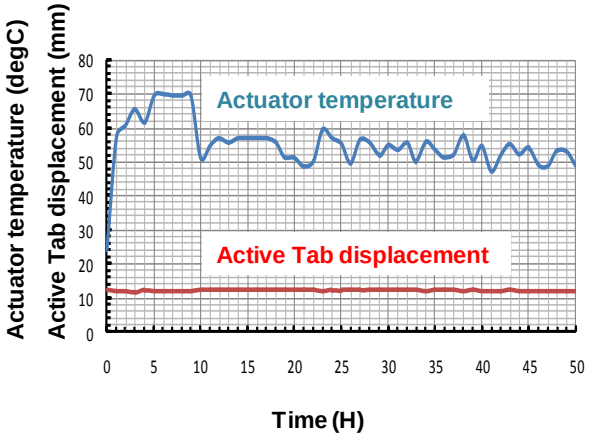

Figure 29: Temporal variation of piezo actuator surface temperature and Active Tab displacement [23]

Input voltage=50V+/-50V
Active Tab frequency=2/rev (43.3Hz)
with 20N simulated lift acted on tab

As shown in Fig.29, Active Tab drive mechanism worked successfully for 50 hours with insignificant temperature increase and deterioration of Active Tab displacement. Fig.29 shows a temporal variation of temperature measured on the surface of the piezo actuator and Active Tab displacement for the 50 hour of the operation. The temperature increases sharply after the activation, saturates to 50-60 degC and hold this value during the operation.
This confirmed that Active Tab drive mechanism has enough durability for the practical use installed in helicopter blades without any adverse characteristics of heat accumulation and the mechanical troubles.

6. CONCLUSIONS

Summarizing the results, the followings are concluded by this study.

1. CAMRAD II model for a rotor system with Active Tab was constructed by the structural design and CFD analysis. The drive mechanism of Active Tab was modeled as a lumped mass, and aerodynamic characteristics were implemented as 2-D airfoil tables with different tab chord lengths. BVI noise characteristics were analyzed using the calculated airloads by CAMRAD II. The analysis defined the requirements for Active Tab and its drive mechanism properties.

2. Variations of the BVI noise characteristics were investigated by applying HHC actuation of Active Tab. 3.3 dB BVISPL reduction could be achieved by 3/rev actuation with 6 mm amplitude and 30 degree control phase angle.

3. The Active Tab drive mechanism is developed so that the requirements defined by the analysis are satisfied.

4. The dynamic test demonstrates that the developed Active Tab drive mechanism achieves 12mm displacement at 2/rev and 3/rev with 20N simulated lift acted on the tab, which satisfies the requirement. Although there are some hysteresis both in 2/rev and 3/rev operations, this hysteresis can be coped with the feedback controls to eliminate during the practical use of Active Tab in the blade.

5. Active Tab drive mechanism worked successfully for 50 hours with a insignificant temperature increase and without the mechanical troubles in the endurance test. This confirmed that the finalized Active Tab drive mechanism has enough durability for the practical use installed in helicopter blades.

References

[1] Splettstroesser, W.R., Lehmann, G., v.d. Wall, B., “Initial Result of a Model Rotor Higher Harmonic Control (HHC) Wind Tunnel Experiment on BVI Impulsive Noise Reduction”, 15th European Rotorcraft Forum, Amsterdam , The Netherlands, September 1989, Paper 01.

[2] Splettstroesser,W.R., Schultz, K-J., Kube , R., Brooks, T.F., Booth, E.R., Niesl, G., Streby, O., “BVI Impulsive Noise Reduction by Higher Harmonic Pitch Control :Results of a Scaled Model Rotor Experiment in the DNW”, 17th European Rotorcraft Forum, Berlin, Germany, September 1991, Paper 61.

[3] Gmelin, B., Heller, H., Philippe, J.J., Mercker, E., Preisser, J.S., “HHC Aeroacoustics Rotor Test at the DNW: The Joint German/French/US HART Project”, 20th European Rotorcraft Forum, Amsterdam, The Netherlands, October 1994, Paper 115.

[23] Gmelin, B.L., Heller, H., Mercker, E., Philippe, J.J., Preisser, J.S., Yu, Y.H., "The HART Programme : A Quadrilateral Cooperative Research Effort", 51st Annual Forum of the American Helicopter Society, Fort Worth, TX, May 1995, pp 695-709.

[5] Murashige, A., Kobiki, N., Tsuchihashi, A., Tsujiuchi, T., Inagaki, K., Yamakawa, E., “Final Report of ATIC Model Rotor Test at DNW”, 57th Annual Forum of American Helicopter Society, Washington, DC, May 9-11, 2001.

[6] Jacklin, S., Blaas, A.,Teves, D., Kube, R., “Reduction of Helicopter BVI Noise, Vibration, and Power Consumption Through Individual Blade Control”, 51st Annual Forum of American Helicopter Society, Fort Worth, Texas, May 9-11, 1995.

[7] Haber, A., Jacklin, S., Simone, G., “Development, Manufacturing, and Component Testing of an Individual Blade Control System for a UH-60Helicopter Rotor”, American Helicopter Society Aerodynamics, Acoustics, and Test and Evaluation Specialists Meeting, San Francisco, CA, January 23-25, 2002.

[8] Jacklin, S., Haber, A., Simone, G., Norman, T., Kitaplioglu, C., Shinoda, P., “Full-Scale Wind Tunnel Test of an Individual Blade Control System for a UH-60 Helicopter”, 58th Annual Forum of American Helicopter Society, Montréal, Canada, June 11-13, 2002.

[9] Fürst, D., Keßler, C., Auspitzer, T., Müller, M., Hausberg, A., Witte, H., “Closed Loop IBC-System and Flight Test Results on the CH-53G Helicopter”, 60th Annual Forum of American Helicopter Society, Baltimore, MD, June 7-10, 2004.

[10] Hasegawa, Y., Katayama, N., Kobiki, N., Yamakawa, E., “Whirl Test Results of ATIC Full Scale Rotor System”, 26th European Rotorcraft Forum, The Hague, The Netherlands, 2000.

[11] Aoyama, T., Yang C., Saito, S., “Numerical Analysis of Active Flap for Noise Reduction Using Moving Overlapped Grid Method”, 61st Annual Forum of the American Helicopter Society, Grapevine, TX, June 1-3, 2005.

[12] Roth, D., Enenkl, B., Dieterich, O., “Active Rotor Control by Flaps for Vibration Reduction – Full scale demonstrator and first flight test results –”, 32nd European Rotorcraft Forum, Maastricht, The Netherlands, 2006.

[13] Straub, F., Anand, V., “Aeromechanics of the SMART Active Flap Rotor” 63rd Annual Forum of American Helicopter Society, Virginia Beach, VA, May 1-3, 2007.

[14] Kobiki, N., Saito, S., “Performance Evaluation of Full Scale On-board Active Flap System in Transonic Wind Tunnel”, 64th Annual Forum of American Helicopter Society, Montreal, Canada, April 29-May 1, 2008.

[15] Lorber, P., O'Neil, J., Isabella, B., Andrews, J., Brigley, M., Wong, J., LeMasurier, P., "Whirl and Wind Tunnel Testing of the Sikorsky Active Flap Demonstration Rotor", 67th Annual Forum of American Helicopter Society, Virginia Beach, VA, May 3-5, 2011.

[16] Bernhard, A., Wong, J., “Sikorsky Active Rotor Control Evaluation of NASA/Army/MIT Active Twist Rotor”, 59th Annual Forum of American Helicopter Society, Phoenix, Arizona, May 6-8, 2003.

[17] Weems, D., Anderson, D., Mathew, M., Bussom, R., “A Large-Scale Active-Twist Rotr”, 60th Annual Forum of American Helicopter Society, Baltimore, MD, June 7-10, 2004.

[18] Wierach, P., Riemenschneider, J., Optiz, S., Hoffmann, F., "Experimental Investigation of an Active Twist Model Rotor Blade under Centrifugal Loads", 33rd European Rotorcraft Forum, Kazan, Russia, September 11-13, 2007.

[19] International Standards and Recommended Practices, ENVIRONMENTAL PROTECTION, Annex16 to the Convention on International Civil Aviation, Volume I Aircraft Noise, Chapter 8 and 11.

[20] Kobiki, N., Kondo, N., Saito, S., Akasaka, T., Tanabe, Y., “An Experimental Study of On-blade Active Tab for Helicopter Noise Reduction”, 30th ERF, France, September 2004.

[21] Kobiki, N., Saito, S., Akasaka, T., Tanabe, Y., Fuse, H., “An Experimental Study for Aerodynamic and Acoustic Effects of On-blade Active Tab”, 31st ERF, Italy, September 2005.
[22] Aoyama, T., Yang, C., Saito, S., “Numerical Analysis of BVI Noise Reduction by Active Tab”, 60th American Helicopter Society Annual Forum, Baltimore, MD, June 7-10, 2004.
[23] Kobiki, N., “Design and Performance Evaluation for Finalized Active Tab Drive Mechanism installed in Mach scaled Model Blade”, 39th ERF, Moscow, Russia, September 2013.
[24] Leishman, J. G., *Principles of Helicopter Aerodynamics*, 2nd Edition, Cambridge University Press, USA, 2006.
[25] Kim, D.-H. and Kim, S.-H., “Design of a Dynamically Scaled Rotor System and Verification of the Blade Properties,” 37th ERF, Gallarate, Italy, September 2011.
[26] Johnson, W., “Rotorcraft Aerodynamics Models for a Comprehensive Analysis,” 54th AHS Annual Forum, May 20-22, 1998, Washington, DC.
[27] Norman, T. R., et al., “Full-scale Wind Tunnel Test of a UH-60 Individual Blade Control System for Performance Improvement and Vibration, Loads, and Noise Control,” AHS 65th Annual Forum, Grapevine, Tx, May 27-29, 2009.
[28] Brentner, K. S., Farassat, F., “Modeling Aerodynamically Generated Sound of Helicopter Rotors,” Progress in Aerospace Science, 2003, Vol. 39, 83-120.
[29] Schmitz, F. H., Rotor Noise, Aeroacoustics of Flight Vehicles: Theory and Practice, Volume 1: Noise Sources, Harvey H. Hubbard, ed., NASA RP-1258, Vol.1, WRDC TR-90-3052, 1991, pp.102-106.
[30] Kobiki, N., Saito, S., “A Conceptual Design of Active Tab for Mach scaled Model Blade Installation”, 36th ERF, Paris, France, September 2010.
[31] Kobiki, N., “Performance Evaluation for Active Tab installed in Mach scaled Model Blade”, 37th ERF, Gallarate, Italy, September 2011.
[32] Kobiki, N., “Design and Performance Evaluation for Enhanced Active Tab Drive Mechanism installed in Mach scaled Model Blade”, 38th ERF, Amsterdam, The Netherlands, September 2012.